AERODYNAMIC RESEARCH APPLICATIONS AT BOEING

ICAS-82-5.7.2

A. L. Nagel
Boeing Commercial Airplane Company
Seattle, Washington

ABSTRACT

This paper will show by several recent examples how aerodynamic research tools and methods have been applied to the design of subsonic commercial transport airplanes. Examples include wing modifications, nacelle integration, vortex generators, and cab design. Some recent high Reynolds number tests in the NASA 0.3-meter Transonic Cryogenic Tunnel are also described

I. INTRODUCTION

Boeing has maintained an Aerodynamic Research Unit for many years as a part of its Commercial Airplane Company Aerodynamic Staff. One major activity of the Research Unit has been the development of advanced computational tools; another has been the acquisition of basic data on airfoils, high lift-sections, and various flow control devices. The Research Unit works closely with development programs to assure that research is effective and applied in the best possible manner. This paper describes some recent activities of the Research Unit, plus several examples of how the research results were used in development projects.

II. AIRFOIL RESEARCH

Boeing has been engaged in the development of airfoils suitable for transport airplanes for many years. Both transonic characteristics and low speed high-lift areas have been extensively investigated. While most of the work is done in Boeing facilities, we have been quick to take advantage of any unique capability provided by other facilities. Recently the .3 meter Transonic Cryogenic Tunnel (TCT) has become operational at the NASA-Langley Research Center. This facility is unique in that airfoil testing can be done at chord Reynolds numbers up to 50 million, which is representative of even the largest existing transports. Attendant to the extremely high Reynolds number and small size of this facility are some difficult and expensive model fabrication problems. Figure 1 shows a Boeing model that has been tested in the TCT. The model chord was 6 inches. The coordinate tolerance was specified as .001 inches, which was achieved except for two localized regions that were .0012 inches out of contour. The model, which was constructed of A268 stainless steel and had 54 pressure taps, performed well. As shown in the photograph, metal disk boundary layer trips were originally affixed to the model at 10 percent chord. These were attached with epoxy and stood up well in the cryogenic test environment. After the initial runs, the trips were removed and further testing was done without trips. The test was conducted in July of 1980 as a cooperative program with NASA. Some results of this test are reported in Reference 1.

The data from the TCT test were of high quality and good repeatability. The measured minimum drag coefficient for the airfoil is shown in Figure 2 as a ratio of the turbulent flat plate skin friction. Also shown on the figure are theoretical calculations using the method of Melnik (Reference 2). Because flow visualization was not possible in the TCT at the time of the test, the position of boundary layer transition could not be established with certainty. However, by comparing the tripped and untripped data, it was concluded that at a Reynolds number of 7.7 million transition was occurring at approximately 10 percent chord. Therefore, the theory is shown for the transition point at 10 percent and at the furthest forward that turbulent flow could exist on an unswept wing of this leading edge geometry. The data fall well within the band given by the two theoretical calculations. For reference, a trend curve based on constant transition Reynolds number is also shown. It is seen that it follows the data well.

We conclude from this test that the TCT is a valuable new facility. Its high Reynolds number capability makes it unique, and removes one major cause of uncertainty in airfoil development. However, the comparison given here shows that the uncertainty due to the unknown location of boundary layer transition limits the exactness of test-theory comparisons. Therefore, it is important that transition detection methods be developed for use in this facility.

III. LOW-SPEED HIGH-LIFT AIRFOIL RESEARCH

The flow over a multi-element high-lift airfoil involves very complicated viscous effects that must be properly accounted for if best performance is to be obtained. Figure 3 illustrates some of these phenomena. The several elements of high lift airfoil configurations each develop boundary layers which in many cases interact with those of adjacent elements. Under the conditions of maximum lift appreciable amounts of flow separation exist on one or all of the elements.

Computational tools are now being routinely used in the development of improved low-speed high-lift configurations. A separated flow calculation procedure by Henderson (Reference 3) combines potential flow, boundary layers, and an approximate separated flow model, and so considers most of the essential features illustrated in Figure 3. In Henderson's method, separations are modeled as non-lifting wakes. Figure 4 illustrates a wake modeling from such calculation and also compares the theory to experiment. As shown, the theory is in excellent agreement with the experimental data for this two-element airfoil. It is also seen that the pressure distribution is much different from that given by potential flow theory.

Figure 5 presents a comparison between experimental and theoretically predicted airfoil lift coefficients. The separated flow theory is seen to predict the actual variation of the lift coefficient data very well, including the prediction of $C_{L\ max}$ and the lift fall-off at higher angles of attack.

As the state of the art improves, increasingly complex boundary layer calculations with advanced turbulence models are being made, and there is a requirement for detailed experimental data to check and extend the theoretical methods. Reference 4 by Brune summarizes some recent theoretical work and comparisons with data by Pot (Reference 5) wherein the details of interacting wake and boundary layer were measured. Figure 6 compares some data from Pot's experiment with the Reference 4 theory. It is seen that although there are some differences in the Reynolds stress between the measured and predicted values, the prediction of the velocity profiles is very good, even in the confluent flow region.

In a Boeing experiment, summarized in Figure 7, boundary layer surveys were obtained on a 4 segment high-lift configuration using hot wire instrumentation, thin film instrumentation, and total pressure probes. The figure shows the installation in the Boeing Research Wind Tunnel (BRWT) together with two typical sets of data. At each boundary layer measuring station, detailed profiles of

velocity and all components of turbulence were measured. The upper data plot shows the interference effect of the traversing device to be negligible. The lower data plot shows a typical well developed confluent boundary layer with a characteristic minimum in the velocity profile near its outer edge. Note the extremely good correlation between the pitot and hot-wire data. This test is discussed in Reference 6.

IV. VORTEX GENERATORS

Since their first application by Boeing on the B-47 airplane, vortex generators have proven to be powerful and useful flow control devices. In efforts to improve our understanding of their proper use, both two-dimensional and swept wing wind tunnel tests have been made with vortex generators.

The two dimensional tests were conducted in a transonic insert for the Boeing Supersonic Wind Tunnel (BSWT). Swept wing tests have been done at the Boeing Transonic Wind Tunnel, and the NASA/AMES 11-foot Unitary Plan Tunnel. A parametric two-dimensional investigation was made wherein the effects of size, shape, position, vortex generator incidence, and spacing were all varied systematically. The test were conducted at a Mach number of .74 with chord Reynolds numbers ranging from 8 to 25 million. Figure 8 shows the model in the BSWT transonic insert. The vortex generators were attached individually with the aid of a jig designed to assure accurate positioning. The size of the vortex generators ranged from 1 percent of the chord (the size recommended in Pearcey's classic paper, Reference 7) to 0.2 percent chord. The latter were only .02 inches high.

Figure 9 shows some results from the parametric test series. The vortex generators are seen to be effective over a wide range of incidence angle in increasing lift. The mechanism for lift increase is a delay of shock-induced separation and a rearward movement of the shock. These data are typical in that a particular vortex generator installation tended to be either effective or ineffective, with little gradation between. However, this is not to say that the drag effects are equally small, and it will be noted that the 15 and 20 degree incidences are best at the highest angle of attack.

The results of the two-dimensional tests for size and location effects are summarized qualitatively in Figure 10. The vertical scale represents both the boundary layer thickness and the vortex generator height. The existence of a filled symbol indicates that a vortex generator of the indicated height and chordwise location was effective in delaying shock-induced separations. The half-filled symbols indicate marginal or inconsistent results.

The data are seen to show good effectiveness even when the vortex generator was appreciably smaller than the boundary layer thickness (the thickness shown here was defined by a 99 percent velocity ratio). Based on these and other test results, the Aerodynamic Research Unit has been recommending smaller vortex generators than previously used.

Figure 11 shows a 3-dimensional vortex generator test in the Ames 11-foot wind tunnel on a 747 configuration. A similar 767 model was also tested. The vortex generators were similar to those used in the 2-dimensional test. Seen in the background of this photo is a wake-imaging survey device which contains a pitot tube connected to a light display. The color of the light is controlled by the pitot pressure and the results are recorded photographically, providing a qualitative map of the flow.

Figure 12 shows several typical wake-imaging survey results. They provide a surprisingly detailed view of phenomena occuring on the wing. For example, in the lower figures, the traces of the individual vortex generators are clearly discernable.

Based in part on the results from these tests and correlations thereof, an effective vortex generator pattern (Figure 13) was developed for the 767 in only a few flight tests. A pitch augmentation control system that had been under consideration was shown to be unnecessary.

V. APPLICATIONS Of CFD

Boeing has made extensive use of computational fluid dynamics for the past many years. Early methods (references 8 through 16) were basically Laplace Equation solvers and hence valid for only subcritical flows or linear supersonic flows. The more recent codes, references 17 through 21, solve the full potential flow equations, often with matched boundary layer solutions, and so are valid for transonic flows as well. However, the linear methods are still extremely useful, being capable of treating more complex configurations than the transonic codes. Current CFD research (References 22 and 23) is aimed at making transonic methods as general in terms of geometry as panel methods are today. Figure 14 shows typical computational models as used by current subcritical and transonic codes.

Figure 15 shows an application of a subcritical panel code to tailor the 757 cab design. The requirement was for maximum commonality with the 767, which has a much larger diameter fuselage. The philosophy was adopted that a good design would not involve any localized regions of supersonic flow, hence the subcritical solution would be valid. Where the subcritical solution indicated regions of velocities greater than sonic, contours would be redesigned. Analysis of the original lines indicated several regions of supersonic flow. After recontouring, with a two-degree droop in the overall nose configuration, plus new keel lines and fairings, the subcritical theory indicated that the flow was everywhere less than Mach number .98, which in our experience is adequate assurance that subcritical flow truly exists. These calculations made it possible to proceed with cab design without waiting for wind tunnel testing. Test results (Figure 16) subsequently confirmed the predictions. There were significant time and cost savings for this design change through the use of CFD.

Figure 17 illustrates some recent engine installations, compared to that for the 707. (The engine sketches are scaled to have the same wing chords.) Previous designs, developed primarily through wind tunnel testing, had indicated that engines should be placed outside a certain boundary indicated by the dashed line. Two recent designs, the 707 CFM56 and the 737-300 would have been severely penalized, perhaps impractical, had it been necessary to adhere to the indicated constraint. However, with the aid of modern CFD tools low drag installations were developed for both, well within the traditional forbidden region. The installations are all the more impressive because both are retrofits, which places further constraints on the design. The 757 and 767 locations are shown for reference.

In addition to the two examples cited above, CFD were used on the 757 and 767 in many detail designs, including the fuselage aft body geometry, vertical fin dorsal, horizontal tail, wing-body fairing and wing strake design, flap track fairing and the high lift system. CFD methods were also used for investigations of wind tunnel wall and mounting system interference. CFD methods aided in excrescense drag control by providing local flow directions, velocity, and boundary layer profiles for more accurate drag assessment.

VI. NACELLE EFFECTS ON MAXIMUM LIFT

Although it was ultimately decided not to proceed with the 707-CFM56 project, sufficient engineering and wind tunnel testing had been done that it was considered worthwhile to flight test the final design. The flight tests showed that the high-speed performance was very good but that a degradation had occured in low-speed $C_{L\ max}$. As illustrated in Figure 18, the reduction in $C_{L\ max}$ was equivalent to an increase in approach speed of 7 knots. No degradation had been observed in the wind tunnel. Interaction of the wing boundary layer and nacelle vortices was suspected.

Further wind tunnel tests were conducted using a flow visualization device like that shown in Figure 11, plus extensive theoretical analyses. Flow visualization clearly identified the wind tunnel flow mechanisms that limited maximum lift: outboard wing flow separation. However, diagnosing the flight behavior had to begin with theoretical calculations, because the outboard wing flow

breakdown prevented wind tunnel study of the inboard flow. Using the methods described earlier in this paper and in Reference 24, the predictions of the local section maximum lift coefficients were made and compared with the experimental span-load distribution. This comparison, shown in Figure 19, indicated that at wind tunnel Reynolds number the outboard portion of the wing was near stall, while similar calculations at full scale Reynolds numbers indicated adequate margin. It was concluded therefore that at the low Reynolds numbers of wind tunnel tests, flow separation on the outboard wing and flap determined the $C_{L\ max}$. At the high Reynolds numbers of flight the outboard wing performed well, and it was unfavorable interactions of the inboard wing boundary layer with vortices shed from the nacelles that was limiting (Figure 20).

The nacelle vortex and boundary layer interaction is much too complex for theoretical models, so a means was needed to make the wind tunnel data represent the flight phenomena. The approach taken is illustrated in Figure 21. The outboard leading edge device was redesigned so as to have a higher maximum lift coefficient in the wind tunnel environment. This redesigned device was of course not geometrically similar to that on the full scale airplane.

As shown in Figure 22, the redesigned leading edge device, when tested, showed a significant increase in outboard region $C_{L\ max}$. In the wind tunnel test with the redesigned leading edge device, the trailing edge separation of the outboard wing was satisfactorily controlled and it was now possible to study the nacelle vortex effects on the inboard wing. The next step was to design a nacelle vortex control device to improve the inboard wing stall characteristics.

The final results of this study are illustrated in Figure 23. The bars on the left hand side of the figure for the baseline configuration are all normalized to unit values. The next group of three bars show the redesigned leading edge effects on the three configurations: no nacelle, large nacelle, and large nacelle with a vortex control device. As shown, the wind tunnel test with the redesigned leading edge now showed a degradation in $C_{L\ max}$ similar to that observed in flight. The third bar indicates that the vortex control device virtually restored the $C_{L\ max}$ loss in the wind tunnel. Finally, the third group of three bars shows that the flight test results are entirely consistent with the wind tunnel data as adjusted for Reynolds number effects.

The final figure shows the CFM56 engines on the 707 airplane in actual flight. The vortex control device and the nacelle vortex produced by it are clearly visible.

VII. CONCLUDING REMARKS

This paper has presented several example applications of tools and methods from the Aerodynamics Research Unit in the Boeing Commercial Airplane Company. The results presented are intended to illustrate the mix of experimental and theoretical methods. We are finding that computational fluid dynamics methods are very effective in interpreting and extending the experimental techniques. The combination of the two approaches has allowed the solution to some very challenging and difficult design problems to be achieved in a timely, efficient, and successful manner.

REFERENCES

1. "High Reynolds Number Tests of a Boeing BAC I Airfoil in the Langley 0.3-Meter Transonic Cryogenic Tunnel," Johnson, W. G. Jr., Hill, A. S., Ray, E. J., Rozendaal, R. A., Butler, T. W., NASA-81922, 1982

2. "Turbulent Interactions on Airfoils at Transonic Speeds—Recent Developments," Melnick, R. E., Computations of Viscous/Inviscid Interactions, AGARD CP 291, 1981.

3. "A Solution to the 2-D Separated Wake Modeling Problem and its Use to Predict $C_{L\ max}$ of Arbitrary Airfoil Sections," Henderson M. L., 1978, AIAA Paper No. 78-156.

4. "Theoretical Predictions of Confluent Boundary Layers," Brune, G. W., Proceedings, Third Symposium on Turbulent Shear Flows, Davis, California, September 1981.

5. "A Wake-Boundary Layer Mixing Experiment", Pot, P. J., Second Symposium on Turbulent Shear Flows, Imperial College, London, July 1979.

6. "Boundary Layer Instrumentation for High-Lift Airfoil Models," Brune, G. W., Sikavi, D. A., Tran, E. T. , and Doerzbacher, R. P., March 1982 AIAA-82-0592, .

7. "Shock-Induced Separation and Its Prevention By Design and Boundary Layer Control," Pearcey, H. H., pp. 1166, Vol. 2, Boundary Layer and Flow Control, 1961.

8. "A Computational System for Aerodynamic Design and Analysis of Supersonic Aircraft," Middleton, W. D., and Lundry, J. L.,NASA Contract NAS1-13732, NASA CR-2715, July 1976.

9. "Analysis and Design of Supersonic Wing-Body Combinations, Including Flow Properties in the Near Field, Part 1—Theory and Application," Woodward, F. A., Tinoco, E N., and Larsen, J. W., NASA CR-73106, 1967.

10. "A Method for Predicting the Stability Characteristics of an Elastic Airplane, Vol. I—FLEXSTB Theoretical Manual," Dusto, A. R., et al., NASA CR114712, 1974.

11. "A General Method for Determining the Aerodynamic Characteristics of Fan-In-Wing Configurations," Vol. I—Theory and Application, Technical Report 67-614, Rubbert, P. E., Saaris, G. R., Scholey, M. B., and Standen, N. M., USAAVLABS, 1967.

12. "A General Three-Dimensional Potential-Flow Method Applied to V/STOL Aerodynamics," Rubbert, P. E., and Saaris, G. R., SAE J., Vol. 77, September 1969.

13. "Review and Evaluation of a Three-Dimensional Lifting Potential Flow Analysis Method for Arbitrary Configurations," Rubbert, P. E., and Saaris, G. R., AIAA Paper 72-188, 1972.

14. "A Higher Order Panel Method for Linearized Supersonic Flow," Ehlers, F. E., et al., AIAA-76-381, July 1976, NASA Contract NAS2-7729.

15. "Advanced Panel-Type Influence Coefficient Methods Applied to Subsonic Flows," Johnson, F. T., and Rubbert, P. E., AIAA-75-50, January 1975.

16. "PAN AIR, A Computer Program for Predicting Subsonic or Supersonic Linear Potential Flows About Arbitrary Configurations Using A Higher Order Panel Method," Vol. 1. Theory Document (Version 1.0), Magnus, A. E. and Epton, M. A., NASA CR-3251, 1980.

17. "A Finite Volume Method for Transonic Potential Flow Calculations," Jameson, A. and Caughey, D. A., Proceedings, AIAA 3rd Computational Fluid Dynamics Conference, 1977.

18. "Recent Progress in Finite Volume Calculations for Wing-Fuselage Combinations," Caughey, D. A., and Jameson, A., AIAA paper 79-1513, 1979.

19. "Grid Generation and Transonic Flow Calculations for Three-Dimensional Configurations," Yu, N. J., Boeing Commercial Airplane Company, AIAA-80-1391.

20. "Transonic Flow Simulations For Complex Configurations With Surface-Fitted Grids," Yu, N. J., AIAA-81-1258.

21. "Transonic Perturbation Analysis of Wing-Fuselage-Nacelle-Pylon Configurations With Powered Jet Exhausts," Wai, J. C. and Yoshihara, H., Abeyounis, W. K., AIAA-82-0255.

22. "Three-Dimensional Transonic Flow Computations Using Grid Systems With Block Structures," Lee, K. D., AIAA-81-0998, 1981.

23. "A Transonic Rectangular Grid Embedded Panel Method," Johnson, F. T., James, R. M., Bussoletti, J. E., and Woo, A. C., Young, D., P., Young, AIAA-82-0953, 1982.

24. "Some Recent Applications of High-Lift Computational Methods at Boeing," McMasters, J. H. and Henderson, M. L., 1981, AIAA Paper No. 81-1657.

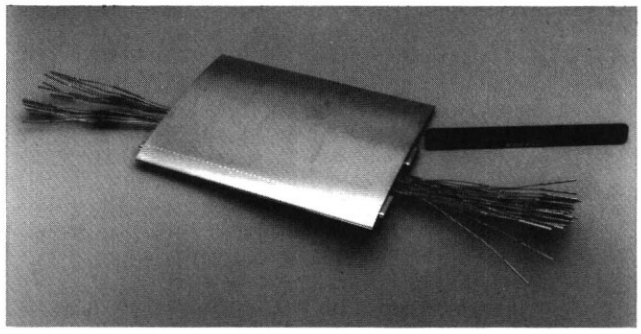

Figure 1. TCT Model

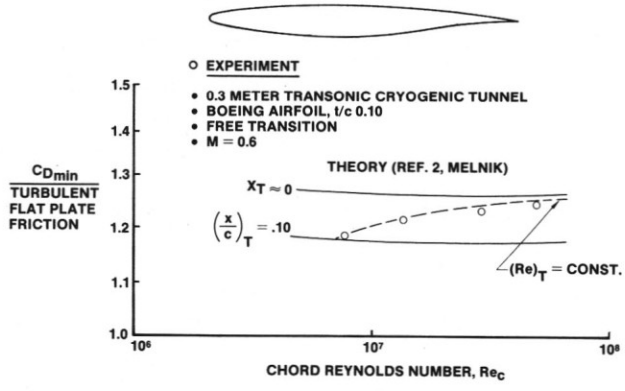

Figure 2. High Reynolds Number Airfoil Test

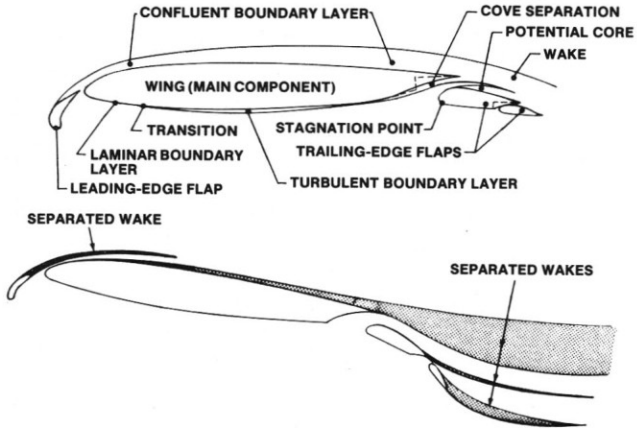

Figure 3. Multi-Element Airfoil Flow Phenomena

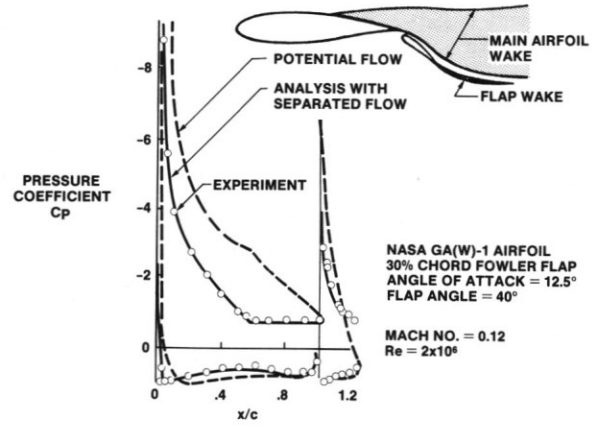

Figure 4. Separated Flow Results for a Two-Element Airfoil

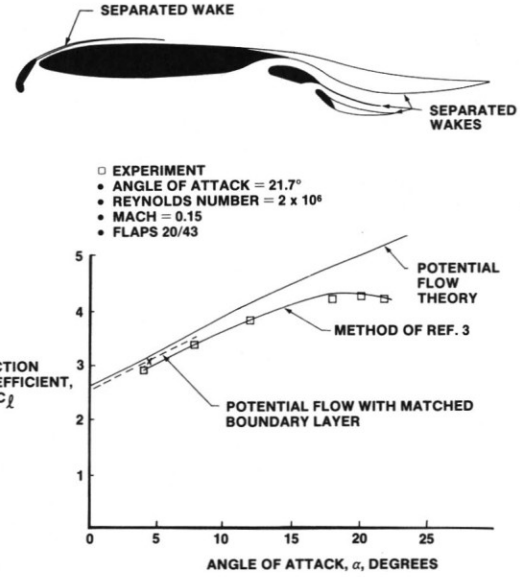

Figure 5. Maximum Lift Prediction vs. Experiment

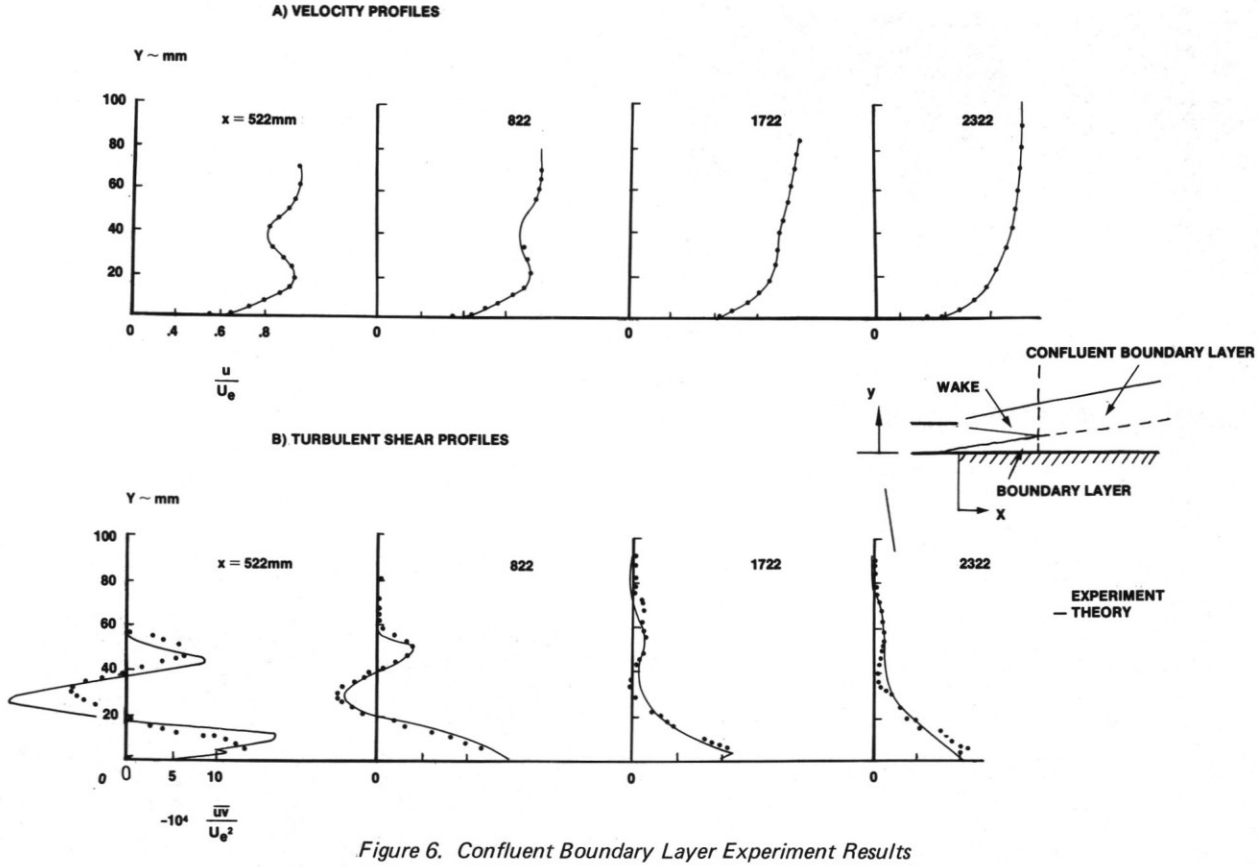

Figure 6. Confluent Boundary Layer Experiment Results

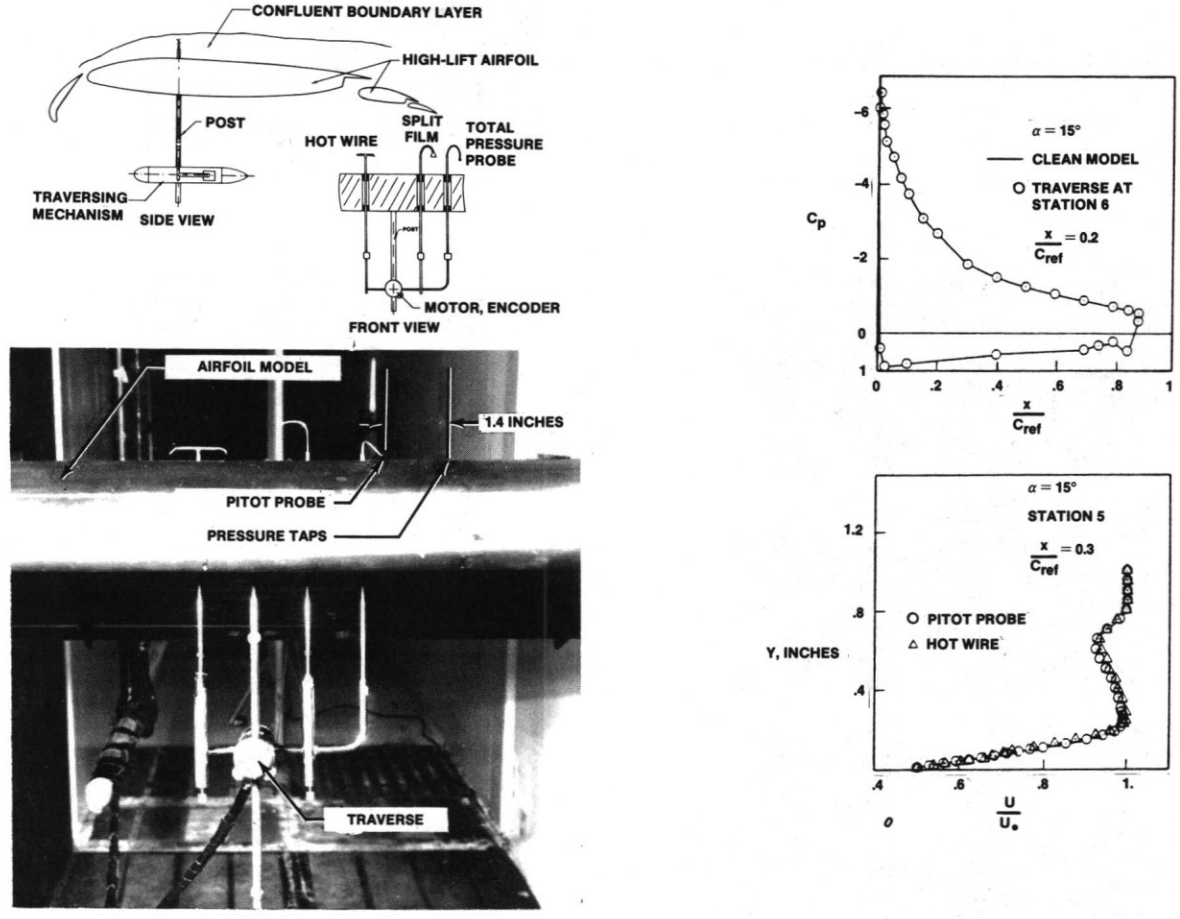

Figure 7. Confluent Boundary Layer Experiment

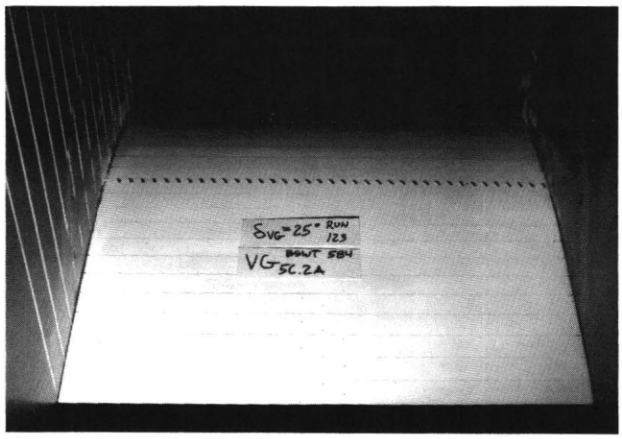

Figure 8. Vortex Generator Test

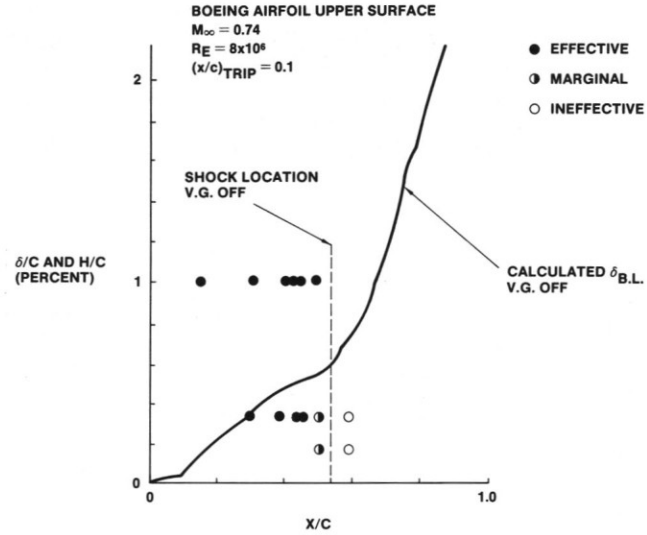

Figure 10. Summary of Results for Co-Rotating Vortex Generators

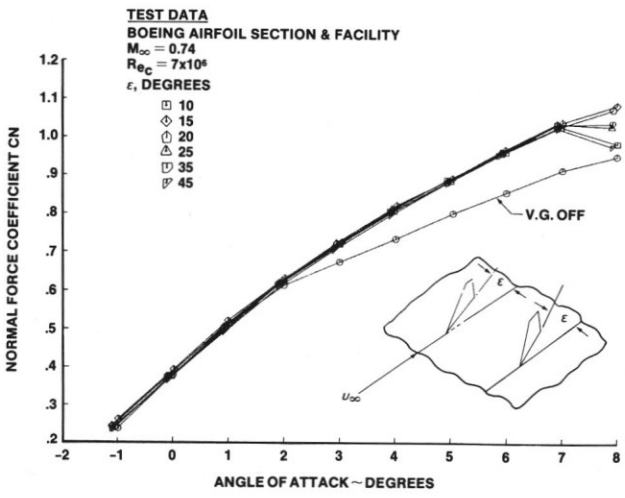

Figure 9. Vortex Generator Effect on Lift

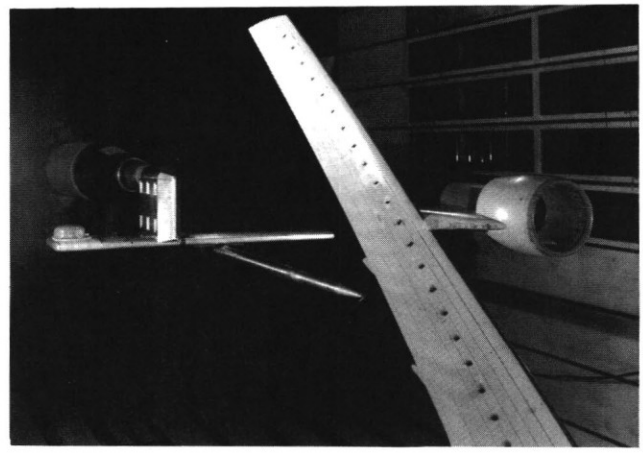

Figure 11. 747 Model With Vortex Generators

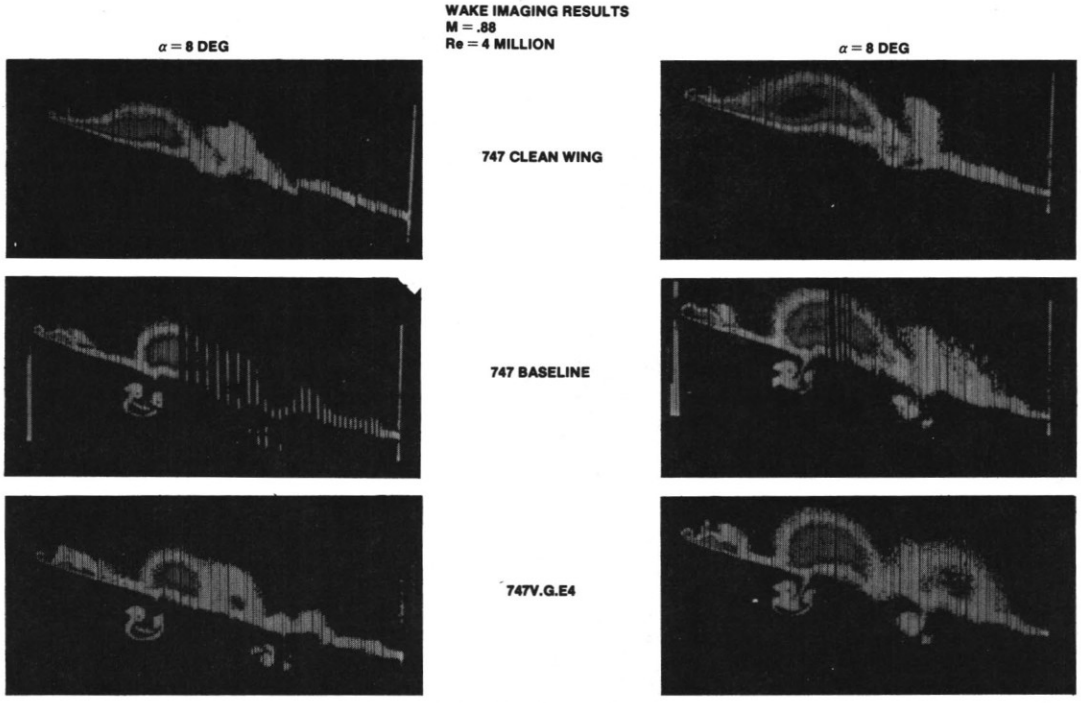

Figure 12. Wake Image Results

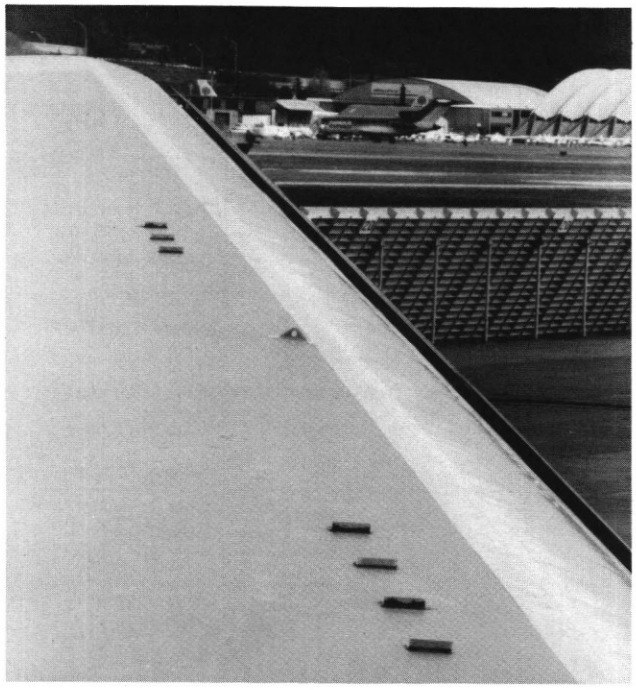

Figure 13. 767 Wing With Vortex Generators.

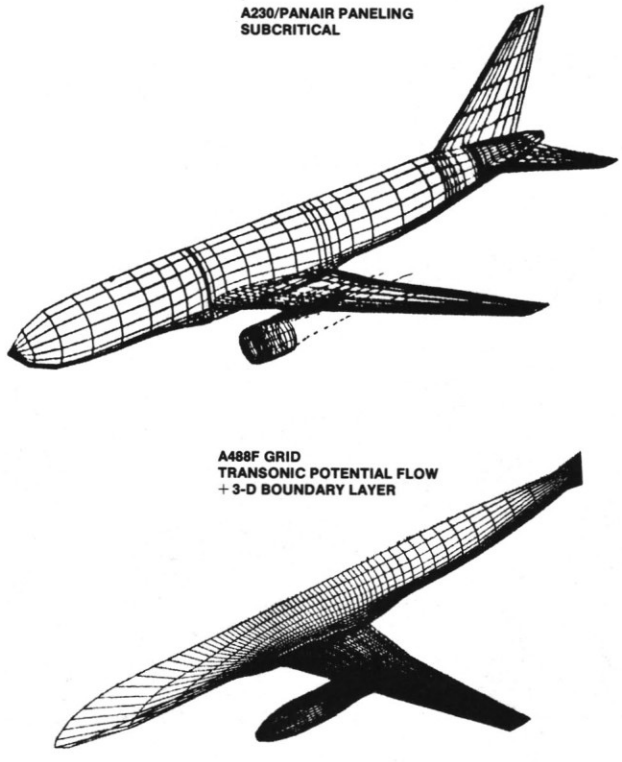

Figure 14. Computational Models

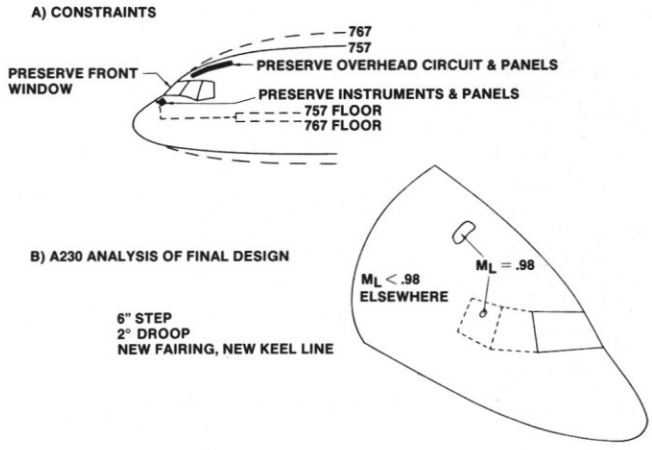

Figure 15. 757 Cab Aerodynamic Design

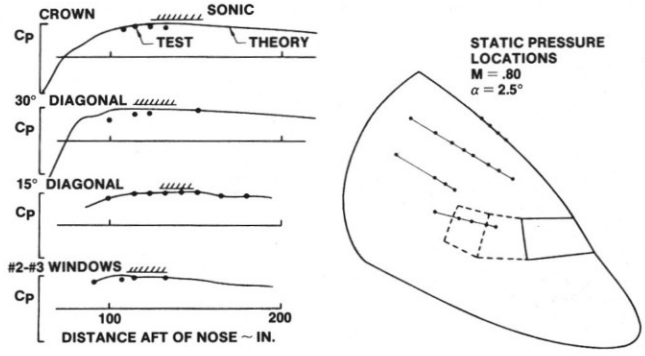

Figure 16. Comparison of Analysis and Test for Cab

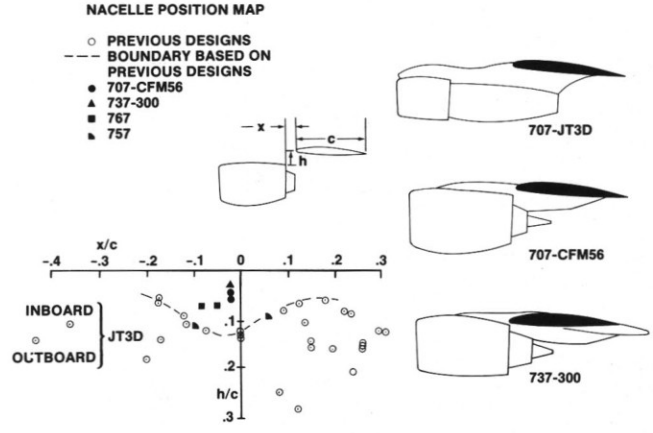

Figure 17. Low Drag Nacelle Installation

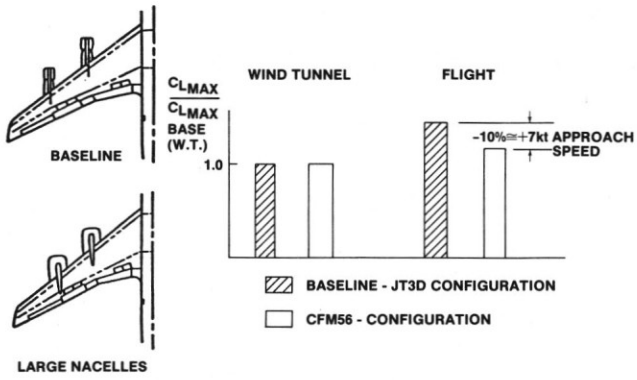

Figure 18. Nacelle Influence on Maximum Lift

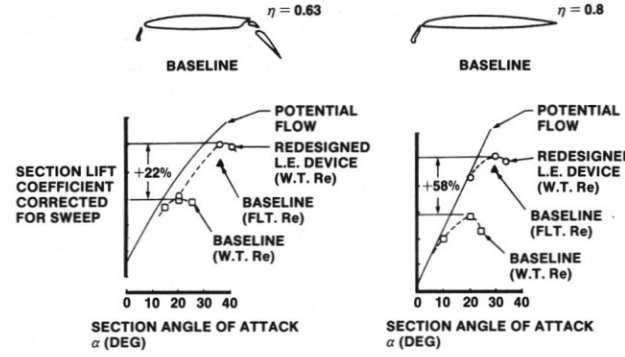

Figure 22. Performance of Redesigned L.E. Device

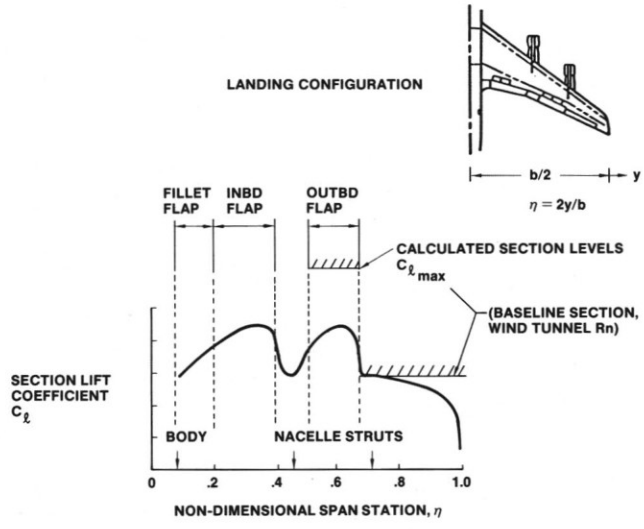

Figure 19. Diagnosis of Wing Maximum Lift Performance

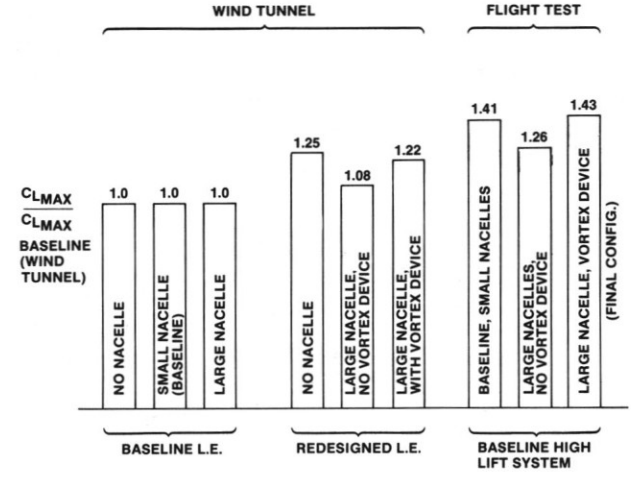

Figure 23. Maximum Lift Comparisons

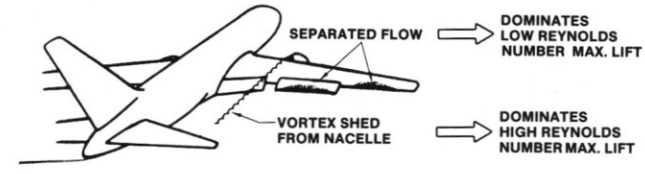

Figure 20. Stall Mechanisms at High and Low Reynolds Numbers

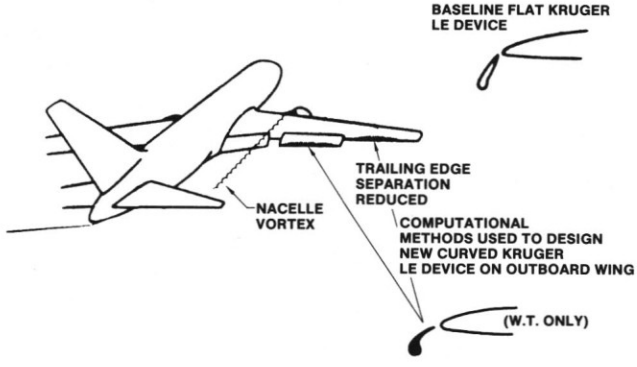

Figure 21. L.E. Redesign Avoids Premature Low Reynolds Number Outboard Stall

Figure 24. 707 CFM56-2 Flight Test Showing Vortex Control Device